μ-Mesonic X Rays in the Iron Region*

C. SCOTT JOHNSON, E. P. HINCKS,† AND H. L. ANDERSON
The Enrico Fermi Institute for Nuclear Studies, The University of Chicago, Chicago, Illinois
(Received October 30, 1961)

The energies and intensities of the μ-mesonic K x rays emitted as muons cascade down through the Bohr orbits of Al, K, Ca, Ti, Cr, Mn, Fe, Co, Ni, Cu, and Zn have been measured as well as the time distribution of K_α x rays from Fe using a NaI spectrometer. This experiment was carried out in an effort to see if some anomaly in the emission of the x rays could help explain the anomalously high muon decay rates reported by Yovanovitch. Such an effect could be explained if for some reason the muons were delayed in reaching the $1s$ atomic level in a time short compared with their lifetime for capture and decay. No effects of magnitude great enough to explain the decay rate anomaly were discovered. The K_α x-ray energies were found to be somewhat higher than those calculated by Ford and Wills. The x-ray yields from the elements studied were found to be close to 100%. From the time distribution of K_α x rays emitted by Fe, an upper limit of 4×10^{-9} sec was set for the mean life of the muons in reaching the $1s$ level.

I. INTRODUCTION

IN the course of some experiments designed to help explain the anomalous decay rates of negative muons bound to nuclei in the region around iron,[1] we measured the μ-mesonic K x rays from these elements. In particular, we wanted to see if the anomaly in the decay rate might be reflected in the μ-mesonic K x-ray yields. If a significant fraction of the negative muons were in some way prevented from reaching the lowest Bohr orbit before decaying or being captured, the anomaly might be explained. An anomalous decrease in the intensity of the K x rays, or a time delay in their emission, would be an indication of such an effect. No such indication was found. However, since our measurements included some elements for which the energies and intensities of the μ-mesonic K x rays had not previously been published, we report them in this paper. Our measurements extend those made earlier, principally by Fitch and Rainwater[2] and by Stearns and Stearns,[3] with some improvements in the technique and in the method of handling the data. Our energy values are precise enough to warrant a meaningful comparison with the careful calculations of Ford and Wills,[4] as will be discussed below.

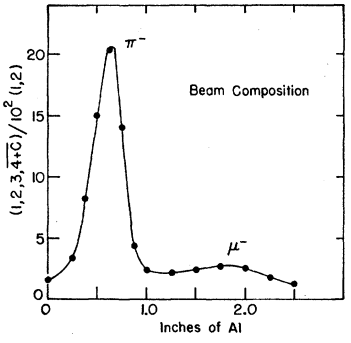

FIG. 1. Differential range curve of the negative 150-Mev/c meson beam used in this experiment. The ordinate gives the relative number of pions and muons stopping in a $\frac{1}{16}$-in. Cu target. In the experiment, pions were absorbed in $1\frac{1}{2}$ in. of Al.

II. ARRANGEMENT

The experiment was performed using the 150-Mev/c negative meson beam of the University of Chicago Synchrocyclotron. This beam emerges from the fringing field of the cyclotron and passes through a 6-in.-diameter vacuum pipe in the 12-ft-thick steel shield which separates the cyclotron from the experimental area. A wedge magnet deflects the beam through 60° and brings it into approximate vertical and horizontal focus at the target of the experimental arrangement. In this experiment the π mesons, which are the principal constituent of the beam, are stopped in an aluminum absorber. A substantial number of electrons contaminate the beam. The interference that these might have caused was greatly diminished by including an electron-sensitive water Čerenkov counter as an anticoincidence element in the beam-defining telescope. The differential range curve of the beam taken with $\frac{1}{16}$ in. Cu between the final coincidence-anticoincidence counter pair of the telescope is shown in Fig. 1. Using these results, we chose $1\frac{1}{2}$ in. of Al to absorb the pions in the experiment.

The counters were arranged as shown in Fig. 2. Counters 1 through 5 were square plastic scintillators attached to Lucite light pipes through which they were viewed with RCA-6810A photomultipliers. Counter C was a water Čerenkov counter used to reject electrons in the beam. The μ-mesonic x rays were detected by counter 6, which consisted of a 5-in.-diam. by 4-in.-thick NaI crystal attached to an EMI-9530B photomultiplier. The NaI counter was placed below the beam to reduce the background from the cyclotron. In addition, it was protected with a lead shield, to reduce background from gamma rays, and a neutron shield consisting of sheet cadmium $\frac{1}{16}$ in. thick (not

* Research supported by the Office of Naval Research.

† On leave from Atomic Energy of Canada, Ltd. Present address: Division of Pure Physics, National Research Council of Canada, Ottawa, Ontario, Canada.

[1] D. D. Yovanovitch, Phys. Rev. **117**, 1580 (1960).

[2] V. L. Fitch and J. Rainwater, Phys. Rev. **92**, 789 (1953).

[3] M. B. Stearns and M. Stearns, Phys. Rev. **105**, 1573 (1957).

[4] K. W. Ford and J. G. Wills, Los Alamos Scientific Laboratory Report LAMS—2387, 1960 (unpublished). This report lists references to all the pertinent experimental and theoretical work on this subject.

shown in Fig. 2), surrounded by a mixture of paraffin and lithium carbonate. Degaussing coils were provided to cancel the vertical component of the cyclotron's fringing field at the photomultiplier. This greatly improved the gain and stability of the NaI counter.

The targets were all 4.8 ± 0.1 g/cm^2 thick and positioned at 45° to the incident beam. Those of denser materials were 4.0 in. square and the dimensionally thick ones were made in the shape of parallelopipeds so that all targets presented to the beam an area 4.0 in. wide by 2.8 in. high. All targets were solid pieces of metal with the exception of Cr, Mn, Co, and Ni, which were powdered metal in thin Lucite boxes.

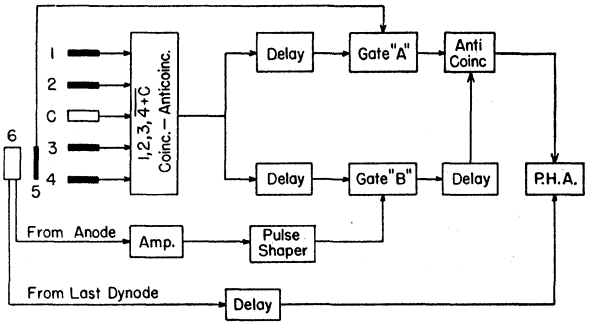

FIG. 3. Block diagram of the electronics.

III. ELECTRONICS

A block diagram of the electronics is shown in Fig. 3. The pulses from all of the telescope counters and counter 5 were amplified by transistor limiting amplifiers and clipped to about 2×10^{-8} sec width before being fed into the telescope coincidence-anticoincidence circuit. A stopping muon produces a $(1, 2, 3, \bar{4}+\bar{C})$ event, where the bar means anticoincidence. Such an event opens two gates, gate A to counter 5, and gate B to counter 6. Counter 6 pulses from the anode of the 9530B photomultiplier were amplified by two Hewlett-Packard 460A amplifiers, then limited by a transistor limiting amplifier and clipped to a width of about 2×10^{-8} sec before entering gate B. Gate B was 5×10^{-8} sec full width at half maximum and when opened allowed the counter-6 pulses to proceed via an anti-coincidence circuit to turn on a 400-channel pulse-height analyzer (Radiation Instrument Development Laboratory model 34–12). In most of the experiment, only 200 channels were employed. Positive pulses from the last dynode of the 9530B photomultiplier delayed by 10^{-6} sec were then analyzed and stored. Gate A enabled a pulse from counter 5 to block a pulse from counter 6 in the anticoincidence circuit. The width of gate A was made three times that of gate B to ensure efficient cancellation of events in which a charged particle passed through both counter 5 and counter 6. These circuits have been described in detail by Gabriel and Segar[5] who developed them in this laboratory.

The response of the pulse-height analyzer was determined to be within $\pm0.2\%$ of perfect linearity (integral) using a precision pulser. The (1,2), (1,2,3) and $(1, 2, 3, \bar{4}+\bar{C})$ counts were monitored during the runs with Hewlett-Packard 520A 10-mc scalers followed by conventional slow scalers.

IV. MEASUREMENTS

Each target was run at least twice in runs of 30 min each, or approximately 10^6 $(1, 2, 3, \bar{4}+\bar{C})$ counts. Targets were changed at the end of each run after a check on the NaI counter gain had been made with a Co^{60} source. The consistency of the Co^{60} calibrations showed no drifts within the accuracy of the count, $\pm0.2\%$. The pulse-height analyzer gain and all other

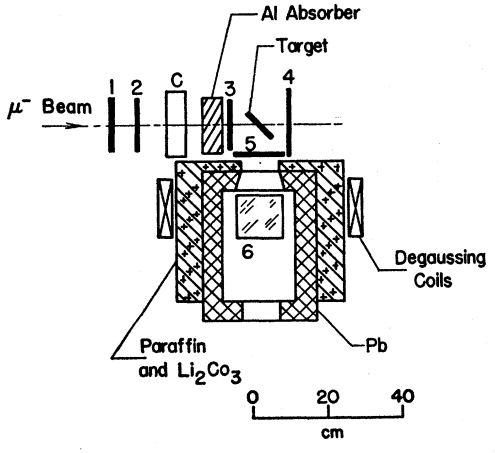

FIG. 2. Side view of the experimental arrangement used for detecting μ-mesonic x rays. Counters 1, 2, 3, 4, and 5 are plastic scintillators. C is a water Čerenkov counter. The NaI detector 6, is situated below the beam level.

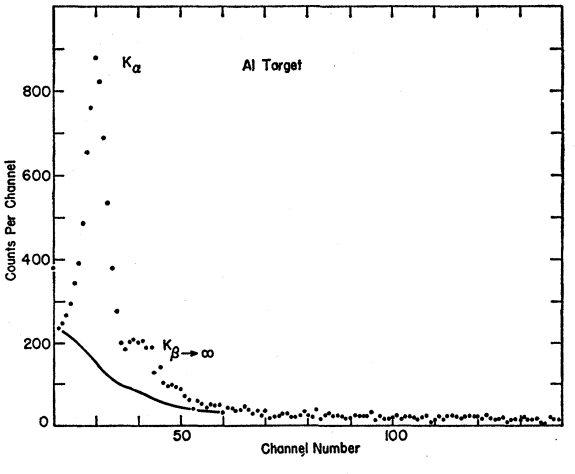

FIG. 4. Pulse-height spectrum of K x rays from Al for 1.15×10^6 $(1, 2, 3, \bar{4}+\bar{C})$ counts. The total Compton and background subtraction is indicated by the solid line.

[5] R. Gabriel and A. M. Segar, Nuclear Instr. and Methods (to be published).

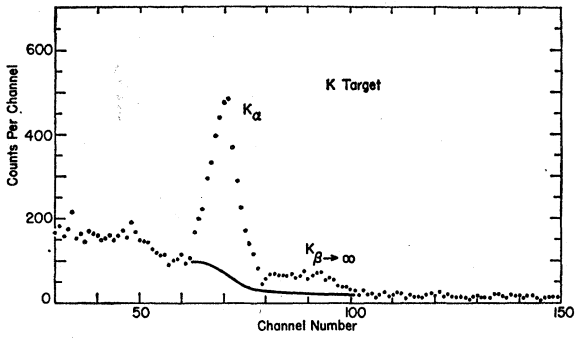

FIG. 5. Pulse-height spectrum of K x rays from K for 1.24×10^6 $(1, 2, 3, \bar{4}+\bar{C})$ counts.

settings were unchanged throughout the experiment except that, to bring Zn within range, the gain was lowered and measurements of Zn and Ti were made in three hours of continuous running for each.

The x-ray spectra obtained are given in Figs. 4 through 14 for each element. The peaks labeled K_α in these figures are due to the x rays from the $2p-1s$ transition. The peaks labeled $K_{\beta\to\infty}$ include the $3p-1s$, $4p-1s$, etc., transitions. The figures also show the estimates of the background and Compton recoil contributions which had to be subtracted in evaluating the photopeaks.

V. DATA REDUCTION

Our reduction of the data was greatly facilitated by the calculations kindly carried out for us by Dr. W. F. Miller of the Argonne National Laboratory. These were Monte Carlo calculations of the energy loss spectra for gamma rays in sodium iodide crystals made for our geometry and our crystal size. The method and calculations for other situations have been given by Miller and Snow.[6] The calculations give the energy loss spectrum for a specified number of incident gamma rays of given energy. From it, one obtains the fraction of x rays that give pulses, the fraction of these within the photopeak and the fraction and distribution of the Compton recoils.

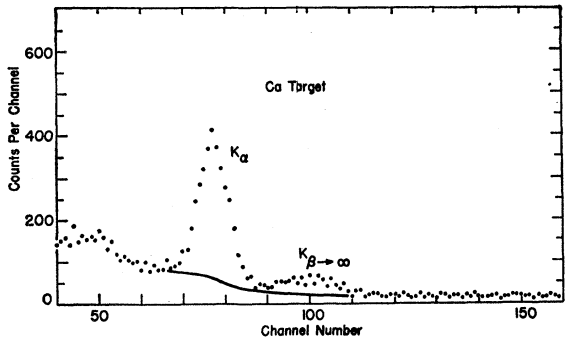

FIG. 6. Pulse-height spectrum of K x rays from Ca for 1.08×10^6 $(1, 2, 3, \bar{4}+\bar{C})$ counts.

In addition to the Compton processes that occur internal to the NaI crystal, there are those that occur external to it, in the target itself, and in the other materials through which the x rays must pass before entering the crystal. These scattering processes distort the shape of the photopeak that is otherwise governed by the finite resolving power of the NaI detector. The number and energy distribution of these scattered x rays may be calculated readily from the Klein-Nishina formula once the electron density in the material traversed is known.

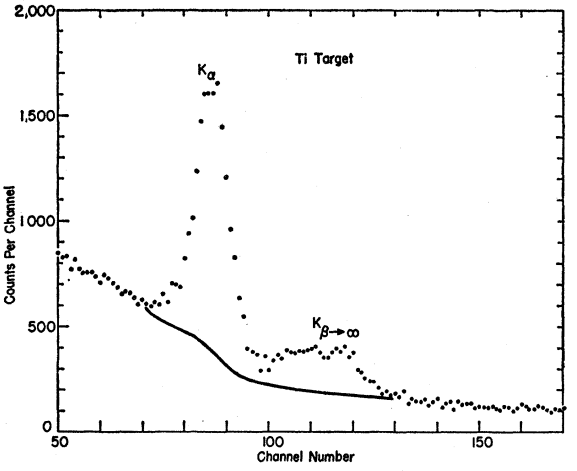

FIG. 7. Pulse-height spectrum of K x rays from Ti for 1.13×10^6 $(1, 2, 3, \bar{4}+\bar{C})$ counts.

In extracting the photopeak from the raw data, we were able to account for all the counts observed as well as their energy distribution as the sum of the

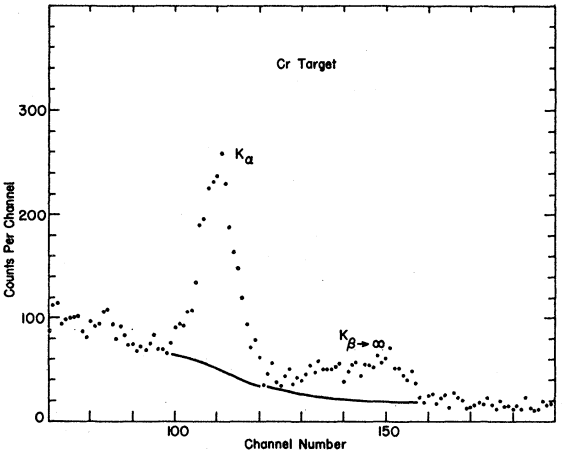

FIG. 8. Pulse-height spectrum of K x rays from Cr for 1.15×10^6 $(1, 2, 3, \bar{4}+\bar{C})$ counts.

[6] W. F. Miller and W. J. Snow, Argonne National Laboratory Report ANL-6318, 1961 (unpublished). Also Rev. Sci. Instr. **31**, 39 (1960).

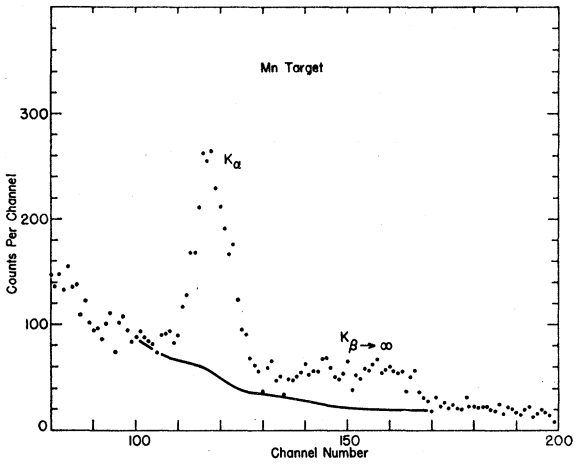

FIG. 9. Pulse-height spectrum of K x rays from Mn for 1.19×10^6 $(1, 2, 3, \bar{4}+\bar{C})$ counts.

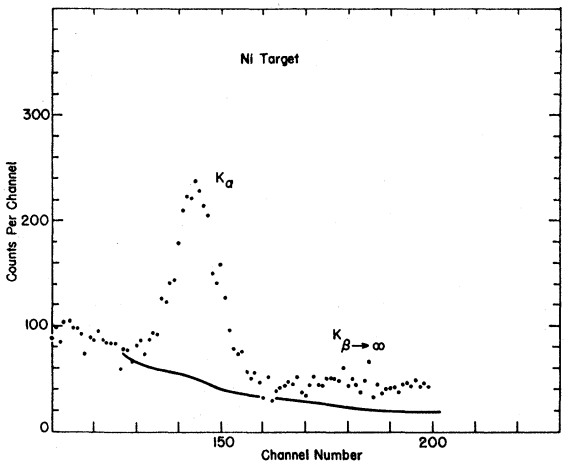

FIG. 12. Pulse-height spectrum of K x rays from Ni for 1.38×10^6 $(1, 2, 3, \bar{4}+\bar{C})$ counts.

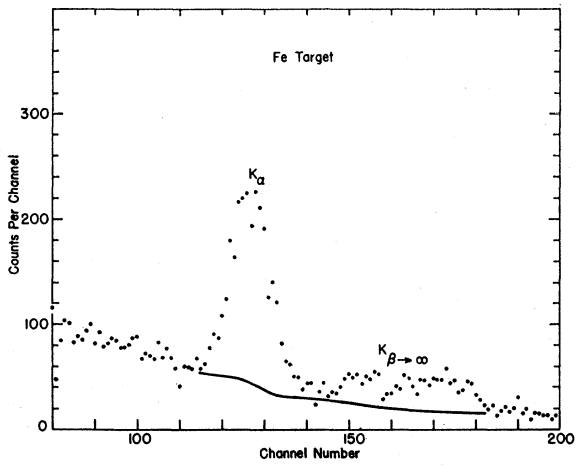

FIG. 10. Pulse-height spectrum of K x rays from Fe for 1.09×10^6 $(1, 2, 3, \bar{4}+\bar{C})$ counts.

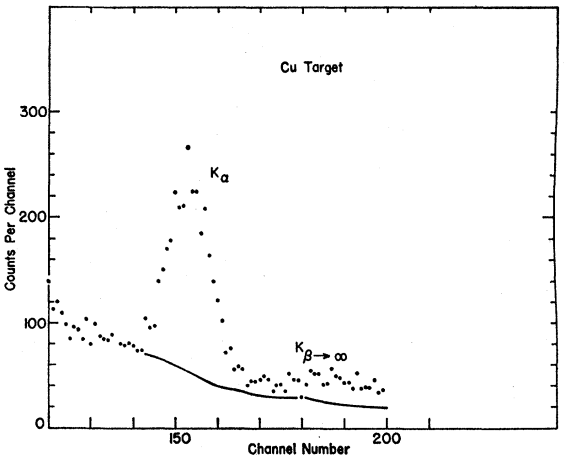

FIG. 13. Pulse-height spectrum of K x rays from Cu for 1.36×10^6 $(1, 2, 3, \bar{4}+\bar{C})$ counts.

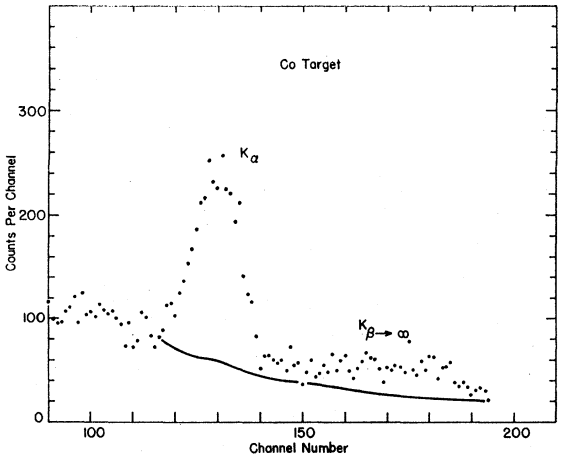

FIG. 11. Pulse-height spectrum of K x rays from Co for 1.47×10^6 $(1, 2, 3, \bar{4}+\bar{C})$ counts.

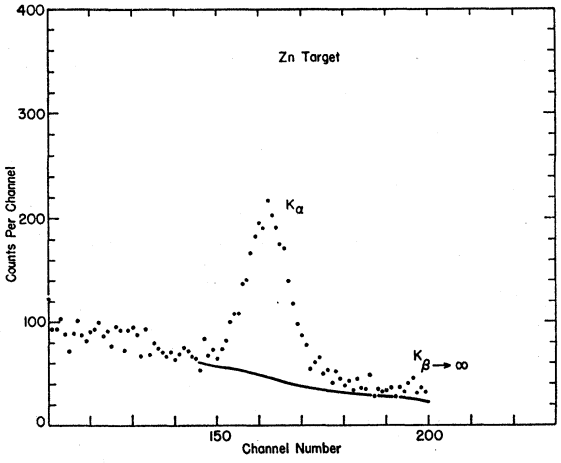

FIG. 14. Pulse-height spectrum of K x rays from Zn for 1.14×10^6 $(1, 2, 3, \bar{4}+\bar{C})$ counts.

following contributions:

(1) background unrelated to μ-mesonic x rays;
(2) x rays scattered by materials external to the NaI crystal;
(3) Compton effect internal to the NaI crystal;
(4) photoeffect in the NaI crystal.

The background was determined from its intensity above the energy of the $K_{\beta\to\infty}$ lines, extrapolating below according to a $1/E$ rule. The validity of this rule was established by verifying that it gave correctly the energy dependence of the background above the $K_{\beta\to\infty}$ lines for the whole series of elements measured in this experiment. In particular, the data obtained with the aluminum target confirmed the rule directly down to 650 kev.

With the background subtracted we could establish, at least approximately, the intensity and shape of the K x-ray lines. We obtained the distribution of counts due to Compton effect internal to the NaI crystal, using the Monte Carlo results, and then the contributions from external Compton scattering using the Klein-Nishina formula. In each case, the observed approximate line shape was folded into the calculated energy distribution as a means of taking into account the finite resolution characteristic of the NaI detector. This procedure was followed first for the $K_{\beta\to\infty}$ lines so as to establish the numbers of counts due to both internal and external Compton processes at the position of the $K_{\beta\to\infty}$ lines as well as below. With these contributions subtracted, the same procedure was followed for the K_α lines. The magnitude of the external Compton contributions calculated from the actual value of the electron density traversed by the x rays was in good agreement with that required to give a good fit to the data well below the K_α line. In extracting the K_α photoline from the data, there were, thus, five subtractions in all; background, internal and external Compton effect from the $K_{\beta\to\infty}$ lines, and internal and external Compton effect from the K_α line itself. The sums of these contributions are indicated by solid lines in Figs. 4 through 14 which give the pulse-height distributions observed. The net counts showed reassuringly sharp and symmetric K_α peaks which could be used with some confidence in the determination of the energies and intensities of the lines.

A typical calculation is given below in Table I for potassium. The second column gives the observed count in the channels of interest; the third gives the background; the fourth gives the contributions from the $K_{\beta\to\infty}$ lines of the Compton recoils within the NaI crystal as obtained from the Monte Carlo calculation after the line shape had been appropriately folded in. The fifth column gives the contributions of Compton scattering of $K_{\beta\to\infty}$ radiations from the material external to the NaI crystal. The sixth and seventh columns list the contributions for internal and external Compton processes, respectively, due to the K_α line. The last column gives the net count after all subtractions. This should contain only the counts in the photopeaks.

TABLE I. Example of data reduction using potassium data.

Channel number	Observed counts	Background	$K_{\beta\to\infty}$ Internal Comptons	$K_{\beta\to\infty}$ External Comptons	K_α Internal Comptons	K_α External Comptons	Net counts
55	114	39	7	5	17	51	−5
56	114	38	8	5	12	51	0
57	92	37	8	5	8	51	−17
58	101	37	8	5	6	50	−5
59	105	36	8	5	4	50	2
60	113	35	9	5	2	49	13
61	94	35	9	5	2	48	−5
62	107	34	10	5	1	47	10
63	168	34	10	6	1	47	70
64	201	33	10	6	1	45	106
65	224	33	10	6	1	43	131
66	296	32	10	6	2	41	205
67	333	32	9	7	2	38	245
68	397	31	8	7	2	35	314
69	439	31	7	7	2	30	362
70	475	30	6	7	2	26	404
71	483	30	5	7	1	20	420
72	370	29	4	6	1	15	315
73	292	29	3	6	1	11	242
74	227	29	2	5		7	184
75	172	28	2	4		5	133
76	141	28	1	3		3	106
77	117	28	1	3		2	83
78	84	27	1	2		1	53
79	47	27		2			18
80	58	27		1			30
81	69	26		1			42
82	71	26		1			44
83	67	26					41
84	67	25					42
85	67	25					42
86	70	25					45
87	59	24					35
88	65	24					41
89	76	24					52
90	59	24					35
91	67	23					44
92	72	23					49
93	75	23					52
94	56	23					33
95	60	22					38
96	54	22					32
97	42	22					20
98	38	22					16
99	39	21					18
100	34	21					13
101	32	21					11
102	21	21					0
103	31	21					10
104	22	20					2
105	22	20					2
106	16	20					−4
107	21	20					1
108	26	20					6

The Klein-Nishina formula was used here in the form which gives the differential cross section per electron per unit energy interval,

$$\frac{d\sigma}{dk'}=\frac{\pi r_0^2}{k^2}\left\{\frac{k'}{k}+\frac{k}{k'}-2\left(\frac{1}{k'}-\frac{1}{k}\right)+\left(\frac{1}{k'}-\frac{1}{k}\right)^2\right\}, \quad (1)$$

where k is the initial energy of the x ray and k' its

energy after scattering, both in units $mc^2=0.511$ Mev. The quantity r_0 is the electron radius and $\pi r_0^2=0.249\times10^{-24}$ cm^2.

Introducing N, the number of electrons per cm^2 traversed, we obtain the scattering function

$$S(k',k)=Nd\sigma/dk'. \quad (2)$$

The resolution function of the detector $R(\Delta k,k)$ was obtained with sufficient accuracy by making a rough subtraction from the observed distributions. The scattering correction was obtained by folding, using the expression

$$H(k'',k)=\sum_{k'} R(k''-k', k')S(k',k)\Delta k', \quad (3)$$

and evaluating the data numerically.

VI. X-RAY ENERGIES

An energy calibration of our NaI counter and associated electronics was made using Co^{60} and Na^{22} sources. These have gamma rays whose energies are in the neighborhood of the K x rays studied here. The spectra from these sources are shown in Figs. 15 and 16. These were taken with the source above the target and NaI crystal so that the gamma rays had to pass through the target to reach the NaI crystal. The analysis of these data was carried out following the same procedure as for the K_α photolines. There was additional material between source and detector in this case and the additional effect of Compton scattering caused by this was taken into account in the manner described above.

The mean pulse height C in the photoline gives a measure of the energy and was calculated from the expression

$$C=(1/N)\sum_i c_i n_i, \quad (4)$$

where n_i is the net number of counts in the photopeak at channel c_i, and $N=\sum_i n_i$ is the total number of the net counts under the photoline.

The statistical error in this was calculated from the gross number m_i of counts in channel c_i and the number subtracted, $s_i=m_i-n_i$; thus,

$$(\Delta C)^2=(1/N^2)\sum_i[m_i+(\Delta s_i)^2](C-c_i)^2. \quad (5)$$

The uncertainty Δs_i in s_i is difficult to assess because of the manner in which s_i is estimated. Examination of our measured spectra and of the derivation of s_i suggests that we know s_i to about the same accuracy that we would have had we been able to measure s_i directly in a separate run of standard duration. We have, therefore, taken $(\Delta s_i)^2=s_i$.

Table II lists the energies and mean channel positions of the various gamma rays used in the calibration at low gain. The uncertainty in the energy is that given in the reference paper and is listed in column 2. The statistical error in the mean channel position is listed in column 4.

The channel position may depend on the rate at which energy is deposited in the NaI crystal. This is measured by

$$W=(1/T)\sum_i c_i m_i, \quad (6)$$

where T is the live time of the analyzer during the counting cycle. This number was considerably higher in the calibration measurements than in the x-ray runs

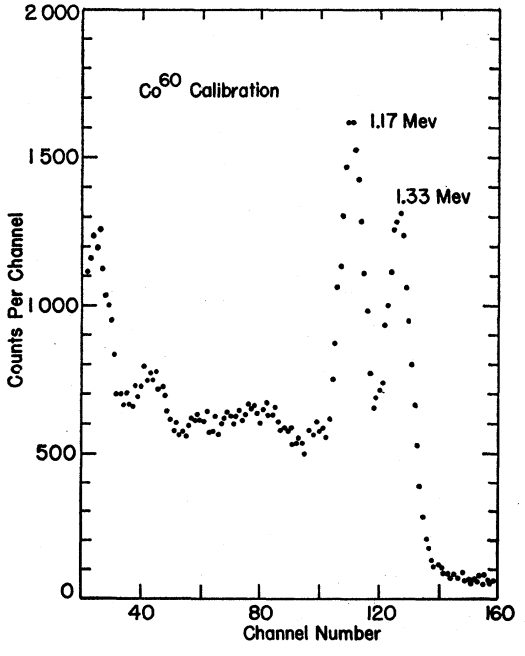

FIG. 15. Pulse-height spectrum of Co^{60} calibration source taken at the low-gain setting.

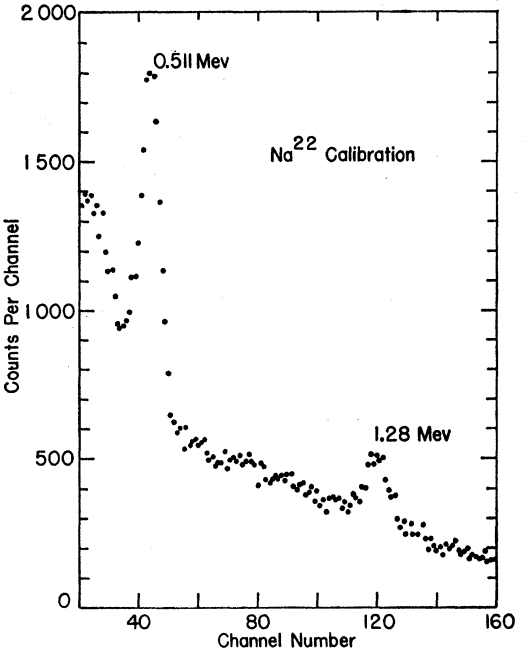

FIG. 16. Pulse-height spectrum of Na^{22} calibration source taken at the low-gain setting.

and gave rise to a shift in the channel position. The magnitude of the shift was evaluated by comparing the mean channel position at various counting rates. The correction is embodied in the channel position listed as C^* in column 5. The total squared error listed in column 6 includes an uncertainty in the magnitude of the shift and an additional uncertainty, other than statistical, in making the subtractions.

A least-squares analysis of the data of Table II, assuming a linear relationship between energy and channel position over the energy range involved, gave the following calibration formula

$$E(\text{kev})=70.4+9.984C, \tag{7}$$

with a mean square error given by

$$(\Delta E)^2=15.5-0.324C+2.09\times10^{-3}C^2. \tag{8}$$

The energies and errors calculated from these formulas for the sources are listed in columns 7 and 8 of Table II, respectively.

This calibration was usable only in the measurements which had been made at the lower gain setting.

In the case of the rest of the data, we had not taken any measurements with the Na^{22} source but could rely on the Co^{60} measurements which were made before and after each run with a different target. In establishing the energy calibration, we included also the channel positions of the Zn and Ti K photolines, since the energies of these had now been determined from the low-gain experiment. The pertinent data, together with the assigned errors, are given in Table III. The least-squares analysis in this case gave the following energy calibration formula:

$$E(\text{kev})=59.6+9.448C, \tag{9}$$

with error

$$(\Delta E)^2=136.7-0.2204C+9.192\times10^{-3}C^2. \tag{10}$$

Using these calibrations, we obtained the energies of the K_α lines given in Table IV. Table IV includes, in the third column, the statistical uncertainty in determining the mean channel position. Insofar as these errors alone are concerned, the channel positions were determined to better than 0.3% in most cases. Other than statistical errors in the subtractions were taken into account by including an additional uncertainty of 0.14 channel in every measurement of the mean channel position. The total error in energy was obtained by adding in quadrature the calibration error [Eqs. (8) or (10)] to these. Column 4 lists all the measurements of μ-mesonic x rays obtained in the present experiment with our best estimate of the errors as discussed above.

As Wheeler[7] had originally pointed out, and as Fitch and Rainwater[2] first demonstrated, the μ-mesonic K_α x-ray energy can be used as a measure of the size of the nuclear charge distribution. However, the measurements of the scattering of high-energy electrons by nuclei carried out by Hofstadter and his collaborators[8] have given a rather precise knowledge not only of the size but also of the shape of the nuclear charge distributions. In view of this, a sufficiently accurate measurement of the μ-mesonic x rays can be used to test the completeness of the theory of the μ-mesonic atoms. Ford and Wills[4] have calculated these K_α energies by solving the Dirac equations with the charge distributions as given by the electron scattering measurements. Their results, including a correction for vacuum polarization, are given in the last column of Table IV. The K_α line is really a doublet, $2p_{\frac{3}{2}}\rightarrow1s_{\frac{1}{2}}$ and $2p_{\frac{1}{2}}\rightarrow1s_{\frac{1}{2}}$. The separation is small (close to 2 kev for Ti) and the

TABLE II. Low-gain calibration data.

Source energy (10 kev)	Uncertainty in energy	Mean channel	Uncertainty in mean channel	C^*	Δ^2	E (10 kev)	$(\Delta E)^2$
51.10	0.00	44.10	0.18	44.13	0.0526	51.10	0.0524
117.28[a]	0.05	109.82	0.14	110.47	0.1446	117.33	0.0521
127.36[b]	0.18	120.75	0.51	120.83	0.3141	127.68	0.0687
133.25[a]	0.03	125.55	0.15	126.29	0.1804	133.13	0.0792

[a] G. Lindström, A. Hedgram, and D. E. Alburger, Phys. Rev. **89**, 1303 (1953); and M. P. Avotina and O. I. Sumbaev, Izvest. Akad. Nauk S.S.S.R. Ser. Fiz. **22**, 879 (1958).
[b] P. P. Singh, H. W. Dosso, and G. M. Griffiths, Can. J. Phys. **37**, 1055 (1959).

TABLE III. High-gain calibration data.

Energy (10 kev)	Uncertainty in energy	Mean channel	Uncertainty in mean channel	C^*	Δ^2	E (10 kev)	(ΔE)
93.59	0.26	92.87	0.25	92.87	0.1477	93.70	0.1134
117.28	0.05	117.66	0.03	118.35	0.1459	117.78	0.0465
133.25	0.03	134.04	0.03	134.83	0.1818	133.35	0.0668
158.67	0.44	161.97	0.40	161.97	0.3771	158.99	0.2090

TABLE IV. Energies of μ-mesonic x rays.

Element	Z	Channel C	Energy (kev) Measured	Theory
Al	13	30.12±0.12	344.2±9.1	344.3
K	19	70.06±0.19	721.5±5.7	702.5
Ca	20	77.19±0.21	788.9±5.3	771.4
Ti	22	92.87±0.25	937.0±4.4	919.8
Ti[a]	22	86.69±0.12	935.9±2.6	919.8
Cr	24	109.53±0.33	1094.4±4.3	1073.8
Mn	25	118.38±0.34	1178.1±4.3	1155.0
Fe	26	126.80±0.34	1257.6±4.3	1238.1
Co	27	134.76±0.32	1332.8±4.3	1323.0
Ni	28	114.19±0.36	1421.9±5.0	1409.9
Cu	29	153.62±0.37	1511.0±5.5	1496.5
Zn	30	161.97±0.40	1589.9±6.2	1586.5
Zn[a]	30	151.88±0.18	1586.7±4.4	1586.5

[a] Calculated from data taken at the lower gain. These energy values were used in the calibration and are not independent of the other measurements in the table.

[7] J. A. Wheeler, Revs. Modern Phys. **21**, 133 (1949).
[8] R. Hofstadter, Ann. Rev. Nuclear Sci. **7**, 231 (1957).

experiment is quite incapable of resolving this fine structure. The tabulation lists the energy differences measured from the center of gravity of the p doublet, i.e., $E(2p)=\frac{1}{3}[2E(2p_{\frac{3}{2}})+E(2p_{\frac{1}{2}})]$. In some cases, we have taken the liberty of carrying out a minor amount of interpolation in order to make the table complete.

Our measured energies are quite close to those calculated by Ford and Wills. In no case is the deviation more than 3%. From the point of view of our original objective, the agreement is good enough. However, a careful study of the errors of the measurement has shown that they are of the order of 0.5%. In view of this, the discrepancy may be real, and the measurements may have more significance than we expected them to have when we undertook the experiment. Actually, in the case of Zn the measured value is in agreement with the theory within the experimental error, 0.3%.

We include a measurement of Al in our results even though it was outside the range of the series of elements under study here. The agreement with theory in the case of Al is good, but the associated error was so much larger than in the other cases that we prefer to exclude this measurement from the following discussion.

The remaining measurements are higher in the average by 1.6% (root-mean-squared value), while the total errors assigned to these measurements average 0.5% (rms value). A detailed comparison of the measurements with the theory is given in Fig. 17. According to Cooper and Henley[9] the correction for nuclear polarization, not included in the work of Ford and Wills, could amount to 1% or more. It may be that most of the discrepancy could be accounted for by this correction. In this case, there is still some question about the trend of the data which shows a decreasing effect with increasing Z, contrary to what would have been expected *a priori*. On the experimental side, we put the greatest reliance on our data in the region near the calibration points centering around Fe. A non-

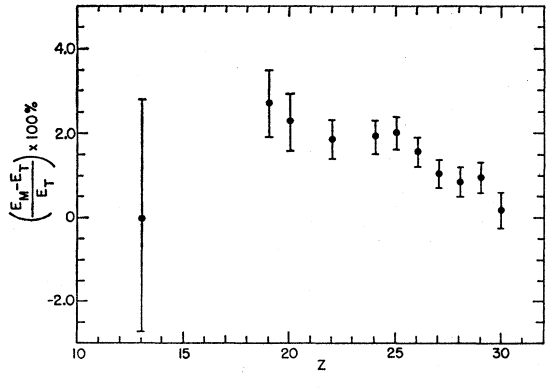

FIG. 17. Plot of the percent deviation of the measured K_α energies (E_M) from the theoretical (E_T) values computed by Ford and Wills.[4] The indicated errors represent the total estimated uncertainties.

[9] L. N. Cooper and E. M. Henley, Phys. Rev. **92**, 801 (1953).

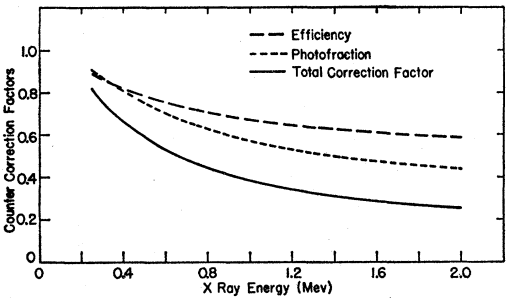

FIG. 18. Plot of NaI efficiency, photofraction, and total counter correction factor. The total counter correction factor is the product of the efficiency and photofractions.

linearity in the response of our NaI detector could produce an artificial trend of the type found here. We have no other basis at present for supposing that the discrepancy in the case of those elements near Fe is not real.

The discrepancy could hardly be due to an error in the value of the nuclear charge radius. According to Ford and Wills, the nuclear charge radius in the case of Ti, for example, would have to be 6% smaller in order to bring the theory 1% closer to agreement with our measurement. This appears to be well outside the range allowed by the electron scattering results. The only other possibility to our knowledge is some anomalous muon-nuclear interaction which has escaped detection thus far.[9a]

Our results are in closer agreement with theory than the original measurements of Fitch and Rainwater. These authors did not, however, specify the accuracy of their measurements, and we cannot make a more meaningful comparison with them.

VII. INTENSITIES

The intensities obtained from integrating the x-ray photopeaks must be corrected for the NaI counter efficiency and photofraction (i.e., the fraction of observed counts in the photopeak). We will refer to these corrections as the counter correction factors. The counter correction factors were obtained from the Monte Carlo calculation referred to above and are plotted in Fig. 18 as a function of x-ray energy.

Corrections were also applied for absorption in the target, in counter 5 ($\frac{1}{4}$-in. plastic scintillator), in the $\frac{1}{16}$-in. cadmium neutron shield, in the $\frac{1}{32}$-in. aluminum

[9a] *Note added in proof.* The calculated K_α energy is sensitive to the shape of the charge distribution chosen in fitting the scattering data. The shape chosen by Hahn *et al.*, yields K_α energies in closer agreement with our results. Moreover, Crannell *et al.*, have shown that this choice is in better agreement with absolute cross-section data. With the bulk of the discrepancy accounted for in this way, residual differences in the energies may be an indication of other nuclear interaction effects.

We have completed a new series of measurements confirming and extending the results given here. [See also B. Hahn, D. G. Ravenhall, and R. Hofstadter, Phys. Rev. **101**, 1131 (1956); H. Crannell, R. Helm, H. Kendall, J. Oeser, and M. Yearian, *ibid.* **121**, 283 (1961)].

TABLE V. Intensities of μ-mesonic x rays.

Element	Normalized α intensity (10^{-6})	Normalized $\beta \rightarrow \infty$ intensity (10^{-6})	Corrected α intensity (10^{-6})	Corrected $\beta \rightarrow \infty$ intensity (10^{-6})	Ratio of $\beta \rightarrow \infty$ to total intensity	Total relative intensity taking Fe=1.000
Al	4086±269	1172±220	7565±680	2266±450	0.230±0.050	0.828±0.069
K	2701±116	686±110	9112±680	2306±390	0.202±0.036	0.961±0.065
Ca	2629±109	537± 89	9244±680	2099±370	0.185±0.035	0.955±0.065
Ti	2325±111	885± 94	8774±680	3716±460	0.298±0.041	1.051±0.069
Ti[a]	1892±119	676±120	7097±620	2837±520	0.286±0.068	0.837±0.069
Cr	1715±100	803±100	6981±590	3567±510	0.338±0.054	0.888±0.065
Mn	1765±104	986± 90	7332±620	4504±500	0.381±0.049	0.996±0.067
Fe	1896±101	832±150	7979±650	3900±600	0.328±0.056	1.000±0.068
Co	1774± 95	825±110	7746±630	4015±590	0.341±0.056	0.990±0.072
Ni	1603± 89	...	7037±580	...	...	...
Cu	1642± 94	...	7458±620	...	...	...
Zn	1487± 86	...	6976±590	...	...	...
Zn[a]	1465± 80	514±120	6806±560	2701±560	0.284±0.064	0.800±0.071

[a] Results of the low-gain runs.

cover on counter 6, and in the $\frac{1}{32}$-in. copper of the NaI crystal container. The absorption corrections[10] are shown plotted vs energy in Fig. 19.

In correcting the $K_{\beta\rightarrow\infty}$ intensities, the energy was taken to be the mean of the calculated K_β and K_∞ energies, respectively.

The results of the x-ray intensity measurements are summarized in Table V. Columns 2 and 3 of the table give the integrated counts in the K_α and $K_{\beta\rightarrow\infty}$ lines normalized to 10^6 $(1, 2, 3, \bar{4}+\bar{C})$ counts. An uncertainty of $\pm 5\%$ was assigned to the magnitude of the subtractions made in obtaining the photopeaks, and this uncertainty has been combined with the statistical uncertainties to give the errors in columns 2 and 3. Columns 4 and 5 give the corrected K_α and $K_{\beta\rightarrow\infty}$ intensities. The errors given in these two columns include a $\pm 5\%$ uncertainty assigned to the counter correction factor and $\pm 2\%$ for each of the two absorption corrections. Column 6 gives the ratio of the $K_{\beta\rightarrow\infty}$ to the total K intensities. The last column gives the total relative K x-ray intensities taking Fe as 1.000. These results are also shown plotted in Fig. 20.

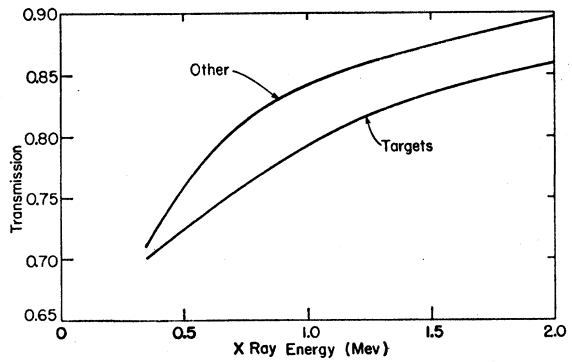

FIG. 19. Data used for correcting x-ray intensities for absorption in the target and in other materials (counter 5, $\frac{1}{16}$-in. Cd, $\frac{1}{32}$-in. Al, and $\frac{1}{32}$-in. Cu).

[10] K. Siegbahn, *Beta- and Gamma-Ray Spectroscopy*, edited by K. Siegbahn Publishers, Inc., New York, 1955), Appendix I, p. 857.

$K_{\beta\rightarrow\infty}$ intensities could not be obtained for Co and Ni because the range of the pulse-height analyzer used was not great enough for the gain setting used in these measurements. The two values listed for Ti and Zn represent the results obtained for the two different gain settings used for these two targets.

The general agreement of the intensity data is consistent with a constant yield of K x rays over the range of Z examined in this experiment.

We did not make an accurate absolute measurement of the yield of x rays per muon stopped. However, we can put our yields on an absolute scale by comparing our results with those of others. The original work of Stearns and Stearns[3] shows the yield of K x rays to be essentially constant at between 80% and 90% above $Z=12$ through $Z=19$, the highest Z reported. More recently, however, Lathrop *et al.*[11] have shown the yield to be close to 100% at $Z=4$ and constant through $Z=7$, the highest Z reported. These results suggest that one should expect a K x-ray yield of close to 100% for Al and K, assuming the Stearns and Stearns results to give the correct relative intensities and the Lathrop *et al.* results to give the correct absolute yields. In view of this, one may conclude that our x-ray intensity measurements are consistent with a yield close to 100% for the K x rays of the elements investigated to an accuracy of about 25%. There is nothing in the behavior here which could account for the Yovanovitch anomaly.

Our results on the fraction of K x rays which are higher than K_α have bearing on the recent calculations by Eisenberg and Kessler.[12] These authors calculated the cascade of μ-mesonic transitions for different initial distributions of states of high n (they use $n=14$). For $Z=14$, they find $K_{\beta\rightarrow\infty}/\text{all } K=0.82$ if only the $14s$ state is populated originally. This falls to 0.36 if the initial distribution of $n=14$ is statistical, each initial state having a weight of $2l+1$. Our results are in best accord

[11] J. L. Lathrop, R. A. Lundy, V. L. Telegdi, and R. Winston, Phys. Rev. Letters 7, 147 (1961).

[12] Y. Eisenberg and D. Kessler, Nuovo cimento 19, 1195 (1961).

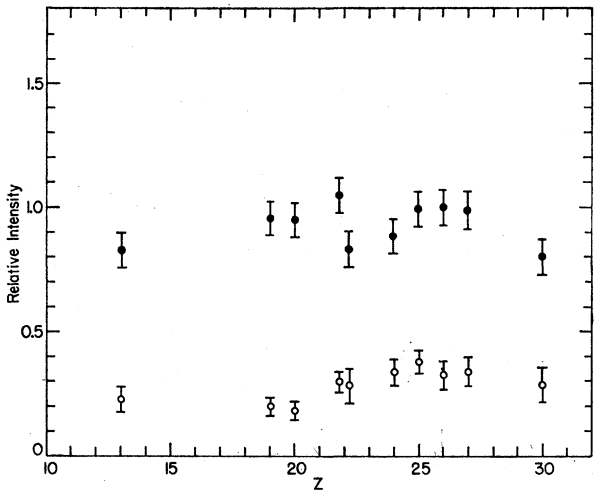

FIG. 20. Plot of the experimentally determined total relative K x-ray intensities (solid dots) taking Fe as 1.000. Also shown plotted here is the ratio of the $K_{\beta\to\infty}$ intensity to the total K intensity (open circles) for the various elements studied. The scale also applies to the intensity on an absolute basis subject to a greater uncertainty as discussed in the text.

with their model of a modified statistical population, more peaked toward the high l values: each state having a weight of $(2l+1)\exp(al)$ with $a=0.2$. In this case, they give $K_{\beta\to\infty}/\text{all}\ K=0.21$ and 0.17 for $Z=14$ and 19, respectively. This compares with our measurements of this ratio, 0.23 ± 0.05 for Al ($Z=13$) and 0.20 ± 0.04 for K ($Z=19$). Thus, states of higher l appear favored in the initial population for these values of Z. Calculations are not given for the higher values of Z covered in our measurements. Here, a trend to increase the relative yield of $K_{\beta\to\infty}$ appears.

VIII. TIME DISTRIBUTION OF K_α X RAYS FROM Fe

In order to measure the time distribution of K x rays, two changes in the electronics shown in Fig. 3 were necessary. Gate B was replaced by a doubles coincidence circuit,[5] and the delayed $(1, 2, 3, \bar{4}+\bar{C})$ pulse into gate B was shortened to 10^{-8} sec by amplification and clipping before making the coincidence with the 6 pulse.

The procedure followed was to take the pulse-height spectrum of the K_α x rays for various $(1, 2, 3, \bar{4}+\bar{C})$ delays. Thirty-minute runs were taken for each delay. The time distribution obtained by integrating the K_α peaks is shown plotted in Fig. 21 vs $(1, 2, 3, \bar{4}+\bar{C})$ delay.

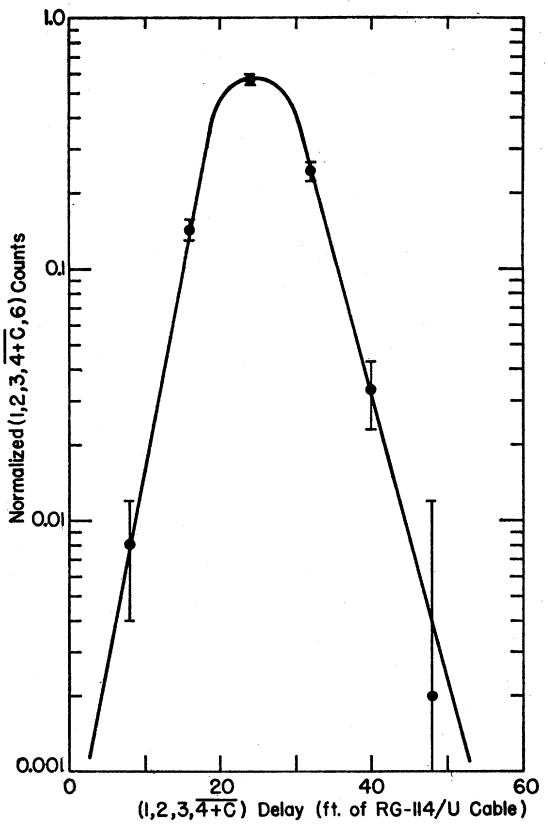

FIG. 21. Time distribution of K_α x rays from Fe.

Analyzing the data by the method of Weaver and Bell[13] gives an upper limit on the mean life of the muon in cascading down through the mesonic Bohr orbits of 4×10^{-9} sec. In analyzing the data, the unknown time resolution function of the apparatus was assumed to be symmetrical.

ACKNOWLEDGMENTS

We are indebted to Dr. W. F. Miller for making the Monte Carlo calculations of the energy loss spectra of gamma rays for our geometry and crystal size which greatly facilitated our data analyses. We would also like to thank C. Rey for his help in the performance of this experiment, R. Gabriel and W. Stanula for their help in the construction of the electronic apparatus, and Professor R. H. Dalitz for helpful discussions.

[13] R. S. Weaver and R. E. Bell, Nuclear Instr. and Methods **9**, 149 (1960).